Computational Mechanics 25 (2000) 207–219 © Springer-Verlag 2000

Dispersive properties of the natural element method

D. Bueche, N. Sukumar, B. Moran

Abstract The Natural Element Method (NEM) is a mesh-free numerical method for the solution of partial differential equations. In the natural element method, natural neighbor coordinates, which are based on the Voronoi tesselation of a set of nodes, are used to construct the interpolant. The performance of NEM in two-dimensional linear elastodynamics is investigated. A standard Galerkin formulation is used to obtain the weak form and a central-difference time integration scheme is chosen for time history analyses. Two different applications are considered: vibration of a cantilever beam and dispersion analysis of the wave equations. The NEM results are compared to finite element and analytical solutions. Excellent dispersive properties of NEM are observed and good agreement with analytical solutions is obtained.

1 Introduction

The Natural Element Method (NEM) (Braun and Sambridge, 1995) is a mesh-free numerical method for the solution of partial differential equations (PDEs). Natural neighbor (*n*-*n*) coordinates (Sibson, 1980) are used as the interpolation functions in the natural element method. Natural neighbor coordinates are based on the Voronoi tesselation of a set of nodes. The optimum spatial adjacency of the interpolation scheme in conjunction with properties such as partition of unity and linear completeness render *n*-*n* interpolation to be a promising choice in a Galerkin method for the solution of PDEs. For a few applications of Voronoi polygons in continuum mechanics, see Cruz and Patera (1982), Ghosh and Mallett (1994), and Cannmo, Runesson, and Ristinmaa (1995).

D. Bueche
Department of Aeronautical Engineering,
University of Stuttgart

N. Sukumar
Theoretical and Applied Mechanics,
Northwestern University

B. Moran (✉)
Civil Engineering, Northwestern University,
Department of Civil and Mechanical Engineering,
2145 Sheridan Rd., Evanston, JL 60208-3109, USA

The authors are grateful for the research support of the National Science Foundation through contract CMS-9732319 to Northwestern University. Helpful discussions with Dr. Mark Christon are gratefully acknowledged.

Braun and Sambridge (1995) introduced natural neighbor interpolation for the solution of partial differential equations. Sukumar (1998), Sukumar, Moran, and Belytschko (1998), and Sukumar and Moran (1999) explored the application of the natural element method for the solution of elliptic boundary value problems that arise in solid mechanics. Here we investigate the properties of NEM within the context of linear elastodynamics. Section 2 is an overview of natural neighbor interpolation. In Sect. 3, the semi-discretized weak form of the governing equation is presented. Applications of the NEM to problems in linear elastodynamics are given in Sect. 4 with particular emphasis on the dispersive properties of the method. The results are compared to finite element and analytical solutions. Finally, some concluding remarks are made in Sect. 5.

2 Natural neighbor interpolation

We briefly touch upon the foundations of Sibson's natural neighbor coordinates (shape functions) that are used in the natural element method. For a more in-depth discussion on the Sibson interpolant and its application to second-order partial differential equations in mechanics, the interested reader can refer to Braun and Sambridge (1995) and Sukumat et al. (1998), and the references therein.

The NEM interpolant is constructed on the basis of the underlying Voronoi tesselation. The Delaunay triangulation is the topological dual of the Voronoi diagram. Within the context of natural neighbor interpolation, the circle that circumscribes a Delaunay triangle is known as a natural neighbor circumcircle (Watson, 1992). In Fig. 1, some of the important geometric constructs associated with a set of nodes are illustrated.

Consider a set of distinct nodes $N = \{n_1, n_2, \ldots, n_M\}$ in $\mathbb{R}^2$. The first-order Voronoi diagram of the set N is a subdivision of the plane into regions T_I (Voronoi cells) given by

$$T_I = \{\mathbf{x} \in \mathbb{R}^2 : d(\mathbf{x}, \mathbf{x}_I) < d(\mathbf{x}, \mathbf{x}_J) \;\; \forall J \neq I\} \;\; , \qquad (1)$$

where $d(\mathbf{x}_I, \mathbf{x}_J)$, the Euclidean metric, is the distance between $\mathbf{x}_I$ and $\mathbf{x}_J$.

The Voronoi diagram for a set of seven nodes is shown in Fig. 2a, and a point $\mathbf{x}$ is introduced into the Voronoi diagram of the set N. If $\mathbf{x}$ is tesselated along with the set of nodes N, then the natural neighbors of $\mathbf{x}$ are those nodes which form an edge of a triangle with $\mathbf{x}$ in the new triangulation. The natural neighbor coordinates of $\mathbf{x}$ with respect to a natural neighbor I is defined as the ratio of the area of overlap of their Voronoi cells to the total area of the Voronoi cell of $\mathbf{x}$ (see Fig. 2b):

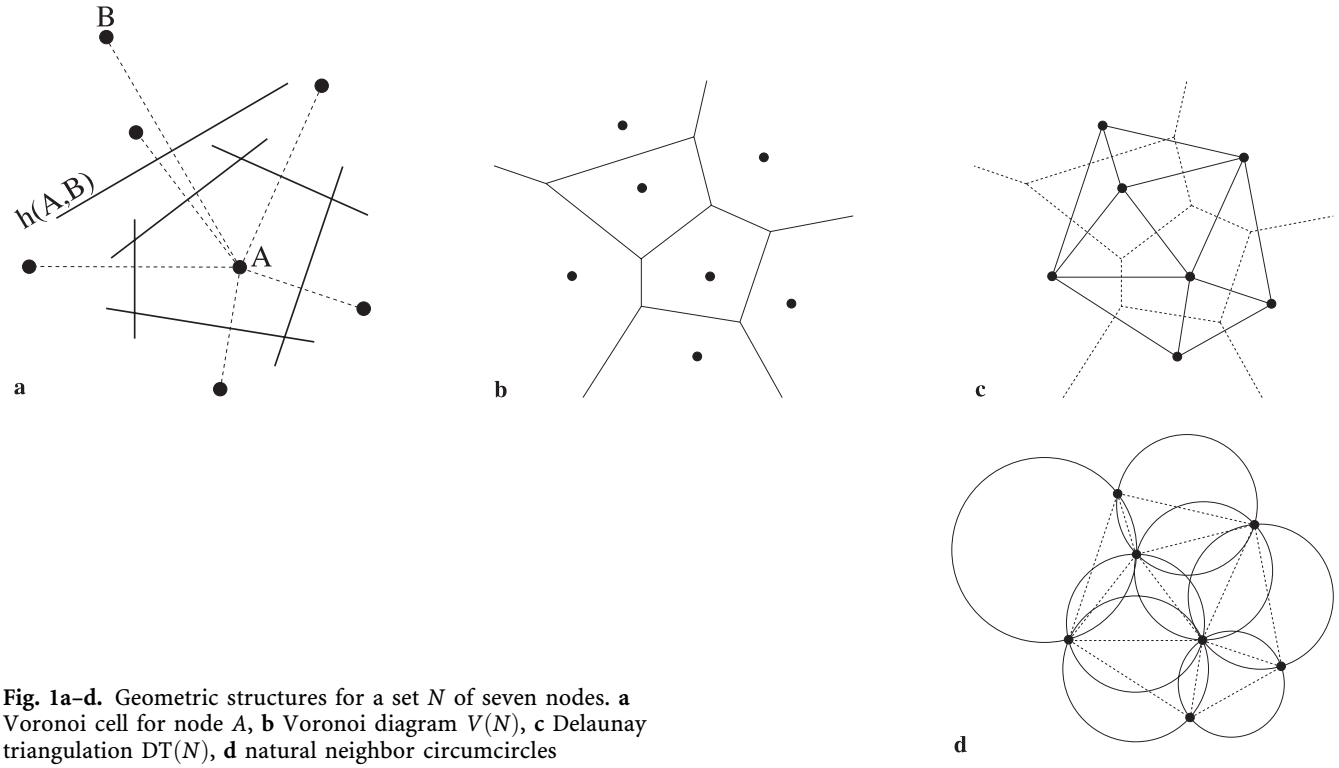

Fig. 1a–d. Geometric structures for a set N of seven nodes. **a** Voronoi cell for node A, **b** Voronoi diagram $V(N)$, **c** Delaunay triangulation DT(N), **d** natural neighbor circumcircles

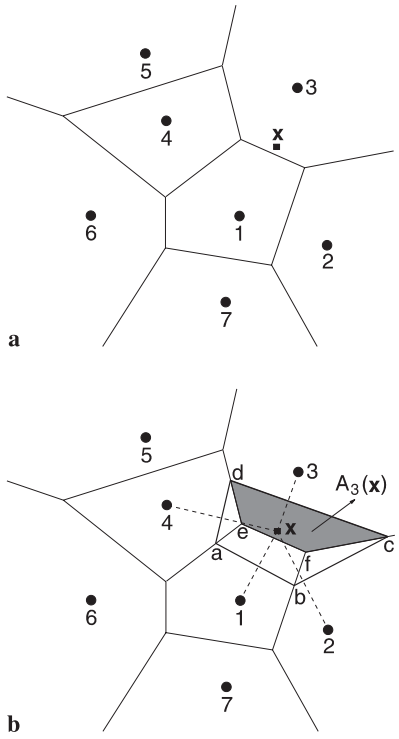

Fig. 2a,b. Construction of natural neighbor coordinates. **a** Original Voronoi diagram and **x**, **b** first-order and second-order Voronoi cells about **x**

$$\phi_I(\mathbf{x}) = \frac{A_I(\mathbf{x})}{A(\mathbf{x})}, \quad A(\mathbf{x}) = \sum_{J=1}^{n} A_J(\mathbf{x}) \tag{2}$$

where I ranges from 1 to n. If the point $\mathbf{x}$ coincides with a node ($\mathbf{x} = \mathbf{x}_I$), $\phi_I(\mathbf{x}) = 1$, and all other shape functions are zero. The properties of positivity, interpolation, and partition of unity directly follow:

$$0 \le \phi_I(\mathbf{x}) \le 1, \quad \phi_I(\mathbf{x}_J) = \delta_{IJ}, \quad \sum_{I=1}^{n} \phi_I(\mathbf{x}) = 1 \ \text{ in } \Omega \ . \tag{3}$$

Natural neighbor shape functions also satisfy the local coordinate property (Sibson, 1980), namely

$$\mathbf{x} = \sum_{I=1}^{n} \phi_I(\mathbf{x}) \mathbf{x}_I \tag{4}$$

which, in conjunction with Eq. (3) imply that the natural neighbor interpolant spans the space of linear polynomials (linear completeness).

On using Eq. (2), we can write the first derivatives of natural neighbor shape functions as

$$\phi_{I,\alpha}(\mathbf{x}) = \frac{A_{I,\alpha}(\mathbf{x}) - \phi_I(\mathbf{x}) A_{,\alpha}(\mathbf{x})}{A(\mathbf{x})} \quad (\alpha = 1, 2) \ . \tag{5}$$

Natural neighbor shape functions are C^∞ everywhere, except at the nodes where they are C^0 (Sibson, 1980; Farin, 1990). The Galerkin implementation of a C^1 natural neighbor interpolant for the biharmonic equation is carried out in Sukumar and Moran (1999). In this study, the geometric algorithm proposed by Watson (1992) is used to compute the natural neighbor shape functions and its derivatives.

Consider an interpolation scheme for a vector-valued function $\mathbf{u}(\mathbf{x})$: $\Omega \subset \mathbb{R}^2 \to \mathbb{R}^2$, in the form:

$$\mathbf{u}^h(\mathbf{x}) = \sum_{I=1}^{n} \phi_I(\mathbf{x}) \mathbf{u}_I \ , \tag{6}$$

where $\mathbf{u}_I$ $(I = 1, 2, \ldots, n)$ are the vectors of nodal displacements at the n natural neighbors, and $\phi_I(\mathbf{x})$ are the shape functions associated with each node. It is noted that Eq. (6) is a local interpolation scheme. The displacement trial and test functions that are used in this paper assume the form shown in Eq. (6).

3
Governing equations and weak form

We consider two-dimensional small displacement elastodynamics governed by the equation of motion. Let $\Omega \subset \mathbb{R}^2$ be a body enclosed by the boundary Γ with unit outward normal $\mathbf{n}$. The equation of motion is given by (strong form)

$$\sigma_{ij,j} + b_i = \rho \ddot{u}_i \quad \text{in } \Omega \ , \tag{7}$$

where σ_{ij} is the Cauchy stress, ρ is the density, b_i is the body force per unit volume, and $\ddot{u}_i$ is the acceleration (material time derivative of the velocity). The constitutive law for small displacements is given by

$$\sigma_{ij} = C_{ijkl}\varepsilon_{kl} \ , \tag{8}$$

where ε_{kl} is the small strain tensor and C_{ijkl} are the material moduli. The kinematic relation between the small strain tensor and the displacement vector u_i is

$$\varepsilon_{kl} = \tfrac{1}{2}(u_{k,l} + u_{l,k}) \ . \tag{9}$$

The essential and natural boundary conditions, and the initial conditions for the strong form are:

$$u_i = \bar{u}_i \ \text{ on } \Gamma_u, \quad \sigma_{ij} n_j = \bar{t}_i \quad \text{on } \Gamma_t \qquad (\Gamma = \Gamma_u \cup \Gamma_t, \ \ \Gamma_u \cap \Gamma_t = \varnothing) \ , \tag{10a}$$

$$\dot{u}_i(\mathbf{x}, 0) = v_{0i}(\mathbf{x}), \quad u_i(\mathbf{x}, 0) = u_{0i}(\mathbf{x}) \ \text{ in } \Omega \tag{10b}$$

where $\bar{u}_i$ and $\bar{t}_i$ are prescribed displacements and tractions, respectively and u_{0i} and v_{0i} are the initial displacements and velocities, respectively. The weak or variational form associated with the strong form is:

Find $u_i \in H^1(\Omega)$ such that

$$\int_\Omega \rho \delta u_i \ddot{u}_i \, \mathrm{d}\Omega = \int_\Omega \delta u_i b_i \, \mathrm{d}\Omega + \int_{\Gamma_t} \delta u_i \bar{t}_i \, \mathrm{d}\Gamma - \int_\Omega \sigma_{ij} \delta \varepsilon_{ij} \, \mathrm{d}\Omega \quad \forall \, \delta u_i \in H_0^1(\Omega) \ , \tag{11}$$

where $H^1(\Omega)$ is the space of functions with square-integrable first derivatives in Ω, and $H_0^1(\Omega)$ is the space of functions with square-integrable first derivatives in Ω and vanishing values on the essential boundary Γ_u. The NEM interpolant is precisely linear on the essential boundary Γ_u (Ω is convex), and hence as in finite elements, the essential boundary conditions can be directly imposed on the boundary nodes (Farin, 1990; Sukumar, Moran, and Belytschko, 1998).

3.1
Matrix form

Consider a Galerkin implementation for the natural element method in two-dimensional linear elastodynamics. The displacement trial functions u_i^h and the test functions δu_i^h are represented as linear combination of natural neighbor shape functions:

$$u_i^h(\mathbf{x}, t) = \sum_{I=1}^{n} \phi_I(\mathbf{x}) u_{iI}(t), \qquad \delta u_i^h(\mathbf{x}, t) = \sum_{I=1}^{n} \phi_I(\mathbf{x}) \delta u_{iI}(t) \ , \tag{12}$$

where lowercase and uppercase indices are used to denote spatial coordinates and node numbers, respectively. The time and spatial derivatives of the trial and test functions are

$$\dot{u}_i^h(\mathbf{x}, t) = \sum_{I=1}^{n} \phi_I(\mathbf{x}) \dot{u}_{iI}(t) \ , \tag{13a}$$

$$u_{i,j}^h(\mathbf{x}, t) = \sum_{I=1}^{n} \phi_{I,j}(\mathbf{x}) u_{iI}(t) \ , \tag{13b}$$

$$\delta u_{i,j}^h(\mathbf{x}, t) = \sum_{I=1}^{n} \phi_{I,j}(\mathbf{x}) \delta u_{iI}(t) \ . \tag{13c}$$

Note that the shape functions are time independent and the nodal displacements u_{iI} are functions of time only. The matrix equation is given by

$$\mathbf{M}\ddot{\mathbf{u}} = \mathbf{f}^{\text{ext}} - \mathbf{f}^{\text{int}} \ , \tag{14}$$

where

$$\mathbf{M}_{IJ} = \int_\Omega \rho \phi_I \phi_J \, \mathrm{d}\Omega, \quad \text{(consistent mass matrix)} \tag{15a}$$

$$\mathbf{f}_I^{\text{int}} = \int_\Omega \mathbf{B}_I^{\mathrm{T}} \boldsymbol{\sigma} \, \mathrm{d}\Omega, \quad \text{(internal force vector)} \tag{15b}$$

$$\mathbf{f}_I^{\text{ext}} = \int_{\Gamma_t} \phi_I \bar{\mathbf{t}} \, \mathrm{d}\Gamma + \int_\Omega \phi_I \mathbf{b} \, \mathrm{d}\Omega, \quad \text{(external force vector)} \tag{15c}$$

where $\mathbf{B}_I$ which is the matrix of shape function derivatives is given by

$$\mathbf{B}_I = \begin{bmatrix} \phi_{I,x} & 0 \\ 0 & \phi_{I,y} \\ \phi_{I,y} & \phi_{I,x} \end{bmatrix} \ . \tag{16}$$

In order to compute the mass matrix, three different approaches are used: consistent mass matrix; row-sum technique which results in a diagonal (lumped) mass matrix; and a lumped mass matrix by using the area of the first-order Voronoi cell to compute its nodal mass.

3.2
Explicit time integration

An explicit central difference time integration scheme is adopted for the temporal discretization of the equations of motion. The maximum stable time step for the central difference method is given by: $\Delta t_{\max} = 2/\omega_{\max}$, where $\omega_{\max}$ is the maximum natural frequency of the system (Cook, Malkus, and Plesha, 1989). For finite elements, Irons and Treharne (1971) showed that $\omega_{\max}$ is bounded by the largest eigenvalue of all single elements of the system. In the case of linear displacement rods, the CFL condition, namely $\Delta t_{\text{ub}} = L/c$, provides an upper bound for the stable time step. However, no such estimate for the stable time step is currently available for the natural element method.

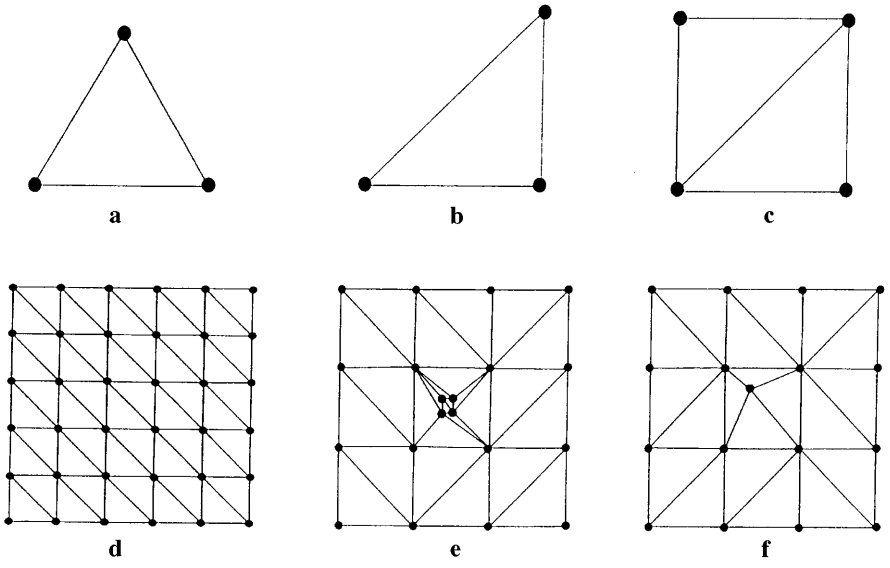

Fig. 3a–f. Nodal discretizations for analysis of stable time step. **a** Equilateral triangle, **b** right-angled triangle, **c** bisected quadrilateral, **d** regular grid, **e** and **f** irregular grids

For lumped mass systems in undamped systems, Gerschgorin's theorem (Isaacson and Keller, 1966) provides a safe upper bound for the stable time step. The theorem is stated as:

$$\omega^{\mathrm{ub}} = \max(\omega_{Ii}) \tag{23}$$

with

$$\omega_{Ii} = \sqrt{\frac{\sum_{J=1}^{N}\sum_{j=1}^{2}|K_{iIjJ}|}{M_{II}}}\ ,$$

where the indices j and J refer to the coordinate direction and the number of nodes, respectively. In addition, K_{iIjJ} are the entries in the stiffness matrix and M_{II} are the diagonal entries in the mass matrix. The upper bound ω^{ub} leads to a safe time step $\Delta t = 2/\omega^{\mathrm{ub}}$ for explicit time integration with the central difference method.

4
Numerical results and discussions

We consider the application of the natural element method to problems in linear elastodynamics. First, estimation of stable time step bounds using a lumped mass matrix are presented. Then, two different problems are numerically solved: cantilever beam under a step load, and dispersion analysis for the first- and second-order wave equations. In the analyses, numerical integration is carried out using a three point symmetric Gauss quadrature rule over the Delaunay triangles. Results are compared to analytical solutions as well as to results obtained using constant strain triangle finite elements.

4.1
Stable time step bounds

The importance of time steps is two-fold in elastodynamics: for linear wave propagation problems, smaller time steps are needed to approximate waves of high frequencies; and in structural dynamics problems time steps play a crucial role for they determine the extent to which the analysis is time intensive. Different approaches for the evaluation of a stable time step have been introduced in Sect. 3.2. Their accuracy for the natural element method is checked by comparing the time step estimates to the exact maximum stable time step which is evaluated by solving the generalized eigenvalue problem: $\mathbf{Kd} = \omega^2\mathbf{Md}$. The time step evaluated by each approach is given as a fraction of the maximum stable time step (Table 1) for the nodal grids shown in Fig. 3. A time step is acceptable if the ratio γ is smaller than one. In the analyses, a lumped mass matrix by the row-sum technique is used.

Table 1. Stable time step bounds for different nodal discretizations

Grids	$\gamma = \dfrac{\omega_{\max}}{(2c/L)}$	$\gamma = \dfrac{\omega_{\max}}{\omega^{\mathrm{ub}}}$
a	1.5175	0.8249
b	1.6054	0.8842
c	1.1952	0.9813
d	1.0278	0.8464
e	0.3178	0.7857
f	0.3138	0.7193

In Table 1, time steps computed using the CFL condition ($\Delta t = L/c$) and the Gerschgorin theorem are presented as a fraction of the maximum stable time step obtained from the eigenvalue analysis. For the time step given by the CFL condition ($\Delta t = L/c$), the ratio γ ranges from about 0.3 to 1.6. The characteristic length L is chosen as the shortest distance between two nodes. Unstable time steps are obtained for the cases (a), (b), and (c) and overly conservative estimates for the graded meshes shown in (e) and (f). Gerschgorin's theorem provides a safe time step bound with ratios from 0.72 to 0.98.

4.2
Cantilever beam

A well-known benchmark problem in structural dynamics is the beam in bending. Consider a cantilever beam subjected to a Heaviside step loading (Fig. 4). The analytical solution for the fundamental time period T of a cantilever beam can be estimated from the classical beam theory as (Hurty and Rubenstein, 1964)

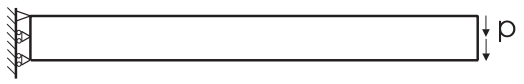

Fig. 4. Cantilever beam problem for fundamental vibration analysis

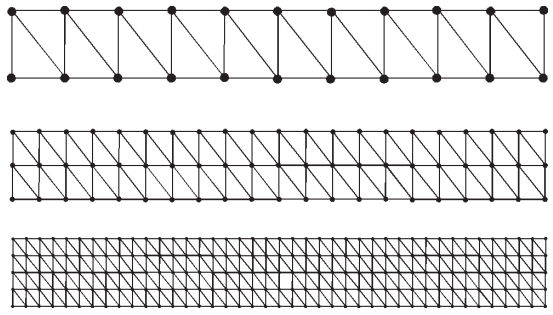

Fig. 5. Nodal discretization for the cantilever beam with 22, 63, and 205 nodes

$$T = \frac{2\pi}{1.875^2}\sqrt{\frac{12\rho l^4}{Eh^2}} \tag{18}$$

where ρ is the density, l is the length, E is the Youngs modulus and h is the height of the beam. The maximum displacement w of the right end of the beam is estimated by calculating the bending deformation. Shear deformation is neglected, due to the chosen geometric relation $l/h = 10$. The maximum displacement is obtained from the equation for static bending with a premultiplied factor of 2 for dynamic loading:

$$w_{\max} = 2\frac{phl^3}{3EI} \tag{19}$$

Using Eqs. (18) and (19), the harmonic vibration of the beam can be written as

$$w(t) = \frac{1}{2}\left[1 - \cos\left(\frac{2\pi}{T}t\right)\right]w_{\max} \tag{20}$$

The cantilever beam is discretized using three different nodal grids with equi-spacing in the coordinate directions (Fig. 5). The time step chosen for the time integration is 0.95 of the critical stable time step: $\gamma = 0.95$. The specimen geometry and material properties are: $p = 1\,\mathrm{N/m^2}$, $\rho = 10\,000\,\mathrm{kg/m^3}$, $E = 210\,000\,\mathrm{N/mm^2}$, $v = 0.3$, $l = 100\,\mathrm{m}$, and $h = 10\,\mathrm{m}$. Plane stress conditions are assumed in the analysis. The analytical solution for the time period and the maximum displacement are $T_{\mathrm{analyt}} = 1.351\,\mathrm{s}$ and $w_{\max} = 3.801 \times 10^{-7}\,\mathrm{m}$, respectively.

Table 2. Fundamental time periods for different nodal discretizations

Method	Number of nodes	T of time integration (s)	T of eigenvalue analysis (s)	Percentage error
NEM	22	1.155	1.144	0.96
	63	1.295	1.306	0.84
	210	1.354	1.343	0.08
FEM	22	0.670	0.684	2.05
	63	1.013	1.026	1.27
	210	1.240	1.239	0.08

Table 3. Time steps for different nodal discretizations

Method	Number of nodes	Stable time step (s)	γ	Number of time steps
NEM	22	2.01E-03	0.95	546
	63	1.05E-03	0.95	1172
	205	5.34E-04	0.95	2409
FEM	22	1.44E-03	0.95	442
	63	7.21E-04	0.95	1335
	205	3.61E-04	0.95	3263

Table 2 compares the fundamental time period obtained using the eigenvalue analysis to that from the NEM semi-discretization. The time integration is carried up to 3000 steps. The results show good agreement between theory and the NEM solution with less then 1 per cent error. The NEM results are markedly better than the constant strain FE results.

In Table 3, the time steps obtained using FEM and NEM are presented. The stable time step decreases with nodal refinement. The stable time steps used in the NEM analyses are approximately 45 per cent greater than their FEM counterparts, which reduces the computing time for time integration by about 30 per cent. In Figs. 6 and 7, the

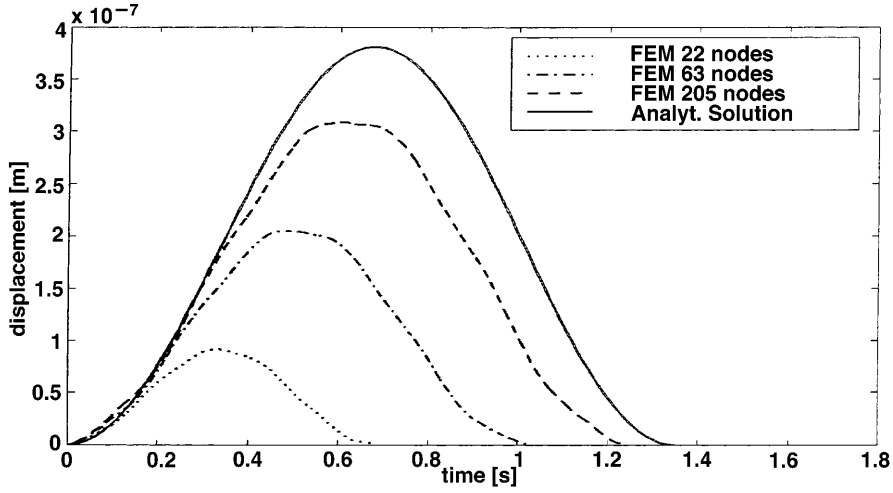

Fig. 6. Fundamental vibration of a cantilever beam with FEM discretization

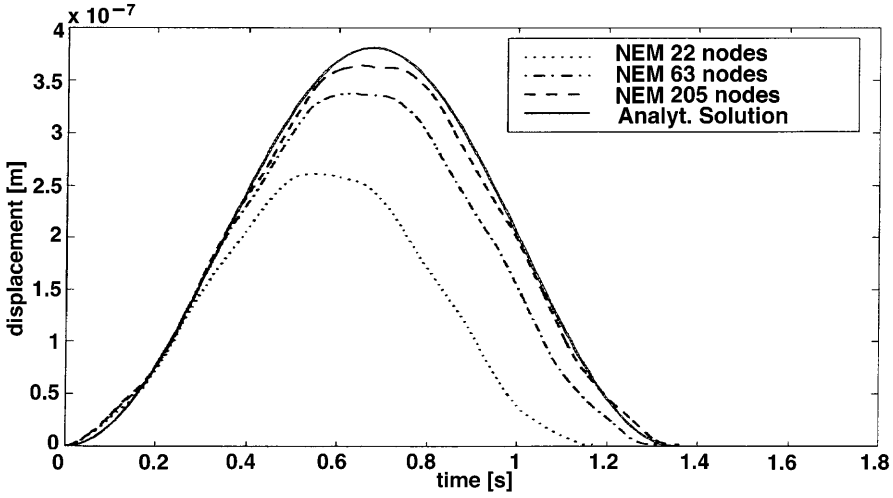

Fig. 7. Fundamental vibration of a cantilever beam with NEM discretization

beam deformation (FEM and NEM) is compared to the analytical solution. There is good agreement between theory and the numerical results. For a given nodal discretization, the NEM solution is significantly better than the corresponding FE solution.

4.3
Dispersion analysis

Dispersion is a phenomenon that occurs in the numerical solution of linear wave propagation problems, even though it is absent in the analytical solution. It is especially pronounced if the wave length is of the same order as the nodal spacing. In this section, the dispersive characteristics of the natural element method are examined for two-dimensional first- and second-order wave equations. Consistent and lumped mass matrix formulations are considered along with different nodal configurations. The NEM results are compared to linear triangular finite elements. Mullen and Belytschko (1982) have carried out a detailed dispersion analysis of the second-order wave equation for linear triangular and bilinear quadrilateral finite elements. Recently, Voth and Christon (1998) have presented a von Neumann analysis for reproducing kernel semi-discretizations. Dispersive phase error is the difference between the numerical phase speed of the wave and that of the analytical solution.

Following Voth and Christon (1998), the two-dimensional first-order (FO) and second-order (SO) wave equations are given by:

$$u_{,x}\cos\theta + u_{,y}\sin\theta + \frac{1}{c}\ddot{u} = 0, \quad \text{(FO)} \tag{21a}$$

$$u_{,xx} + u_{,yy} - \frac{1}{c^2}\ddot{u} = 0, \quad \text{(SO)} \tag{21b}$$

where u is the unknown variable, t is the time, c is the wave speed and θ characterizes the propagation direction of a plane wave measured from the x-axis.

We compare the dispersive properties of the NEM semi-discretization to those obtained for constant strain finite elements. Consistent and lumped mass matrices are considered with uniform nodal spacing in the coordinate directions. In the case of uniform nodal discretizations, lumped mass matrices by the row-sum technique are identical to those computed using the area of the Voronoi cells. Results are plotted as a function of the wave number k and the wave propagating direction θ. Two plots, one circular and the other Cartesian are shown to indicate the dependence of the dispersion on the propagation direction and the wave number, respectively. The polar plots show phase speed as a function of the propagation direction θ, for several values of non-dimensional wavelength, $2\Delta x/\lambda$. The non-circular phase speed contours emphasize the anisotropic nature of wave propagation on the discrete nodal grid. The dispersion analysis follows that given by Voth and Christon (1998) for the reproducing kernel particle method and is not repeated here.

4.3.1
First order wave equation

The normalized phase speed for the NEM and linear FE triangles are shown in Figs. 8–15. A quadrilateral nodal configuration and a hexagonal nodal configuration are examined with consistent and lumped mass matrices. The nodal configuration used in the analysis is indicated in the figure. In general, the dispersion error increases with increasing non-dimensional wavelength, $2\Delta x/\lambda$. Figure 8 shows the NEM results for consistent mass matrix and quadrilateral nodal spacing. The dispersive error is negligible for $\lambda > 5\Delta x$, and the relative wave speed Ψ drops rapidly for $\lambda < 5\Delta x$. The dispersive error is dependent on the propagation direction with maximum error along the coordinate directions. The propagation is periodic in θ with a period of $\pi/2$. The corresponding plot for FEM (Fig. 9) shows larger dispersion error and highly anisotropic propagation, with θ-periodicity of π. Mass lumping leads to larger phase speed errors (Figs. 10 and 11). The natural element method shows excellent isotropy for the lumped mass case (Fig. 10), which is markedly better than that for the consistent mass (Fig. 8). Significantly better propagation properties are obtained for hexagonal nodal configurations (Figs. 12–15), with periodicity in θ of $\pi/3$. Both the NEM and FEM results show better isotropic behavior for the hexagonal nodal configuration than for the quadrilateral nodal configuration.

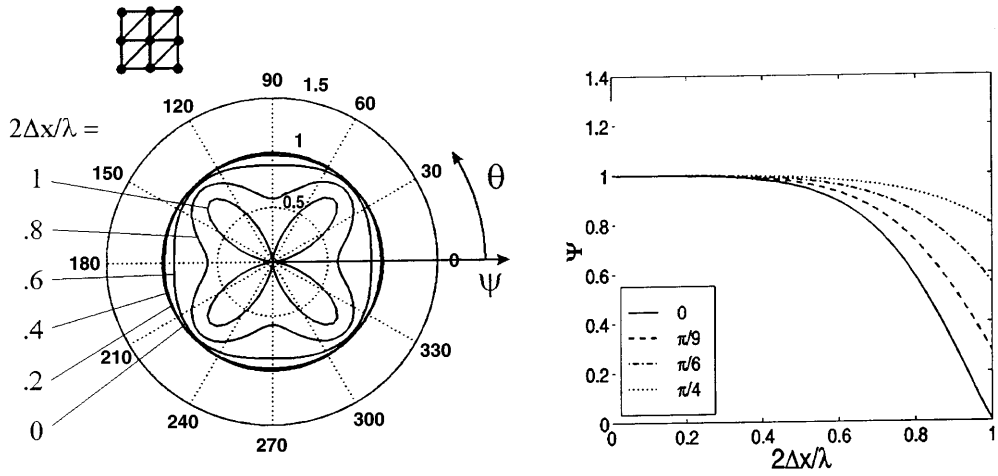

Fig. 8. NEM: First-order wave equation with consistent mass matrix and quadrilateral nodal configuration

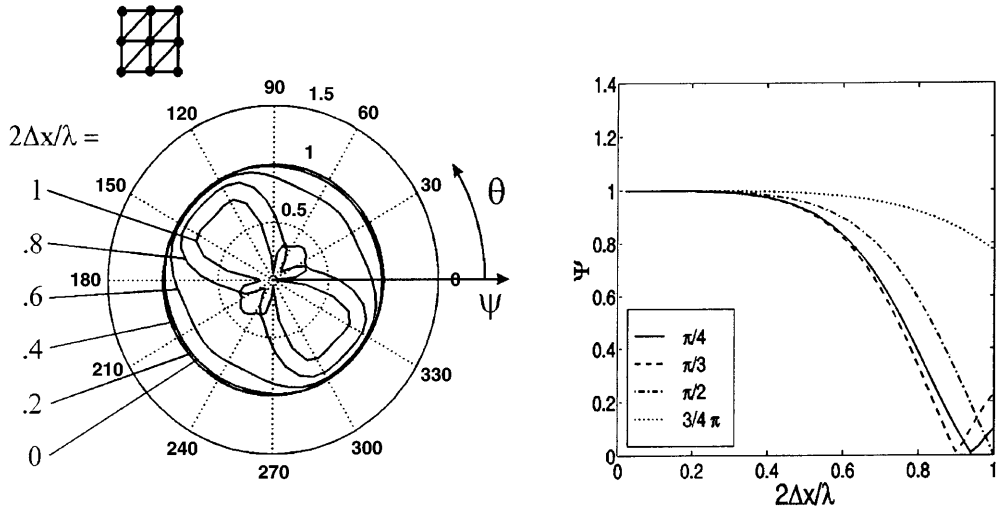

Fig. 9. FEM: Phase speed for the first-order wave equation with consistent mass matrix and quadrilateral nodal configuration

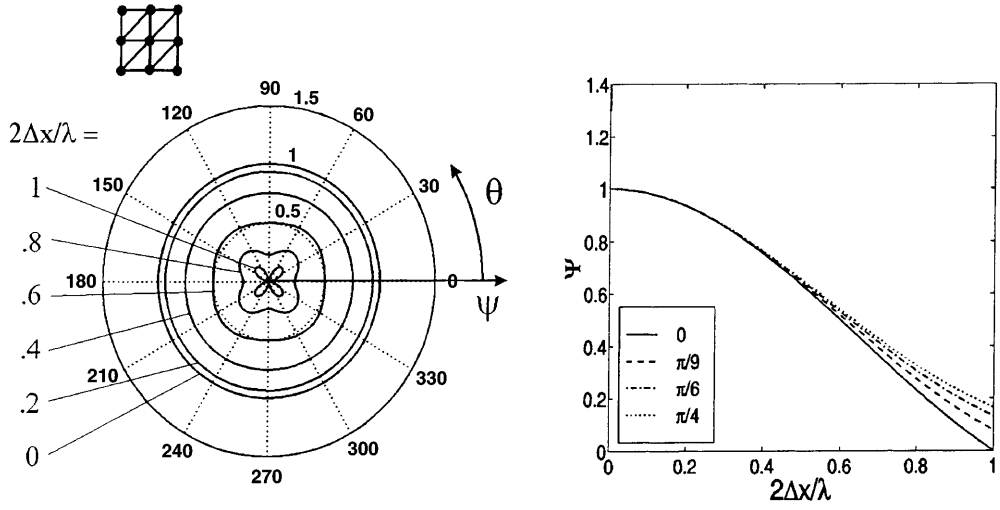

Fig. 10. NEM: Phase speed for the first-order wave equation with lumped mass matrix and quadrilateral nodal configuration

4.3.2
Second order wave equation

The normalized phase speed for the NEM and linear FE semi-discretizations of the second-order wave equation are shown in Figs. 16–23. The numerical characteristics of the phase speed errors for the second-order wave equation are different from the first-order wave equation. In the first-order semi-discretization, the numerical phase speed is always lagging with less deviation for consistent mass matrices. In the second-order case, consistent mass matrices cause leading phase speeds and lumped mass matrices result in lagging ones. Thus the possibility exists of reducing phase errors by balancing the effects of the consistent and lumped mass matrices. The maximum phase error for

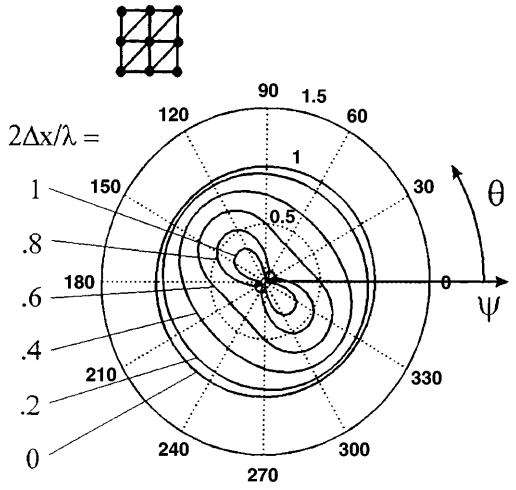

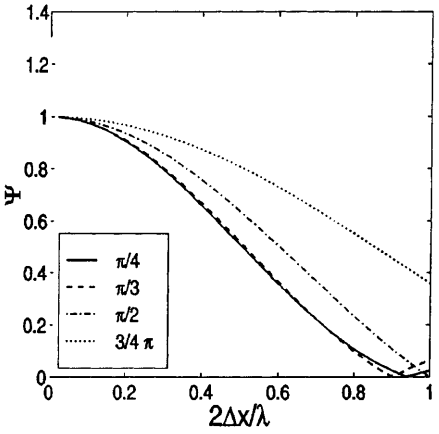

Fig. 11. FEM: Phase speed for the first-order wave equation with lumped mass matrix and quadrilateral nodal configuration

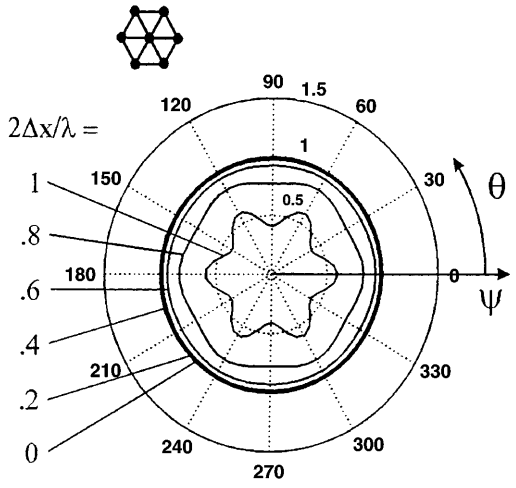

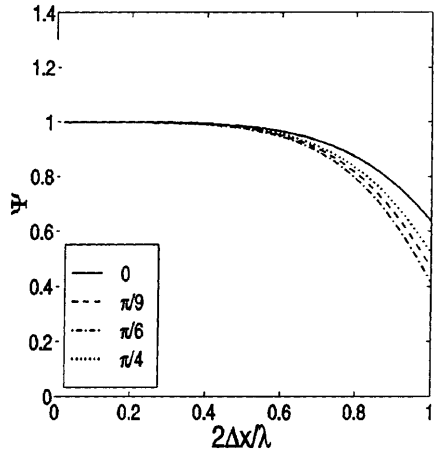

Fig. 12. NEM: Phase speed for the first-order wave equation with consistent mass matrix and hexagonal nodal configuration

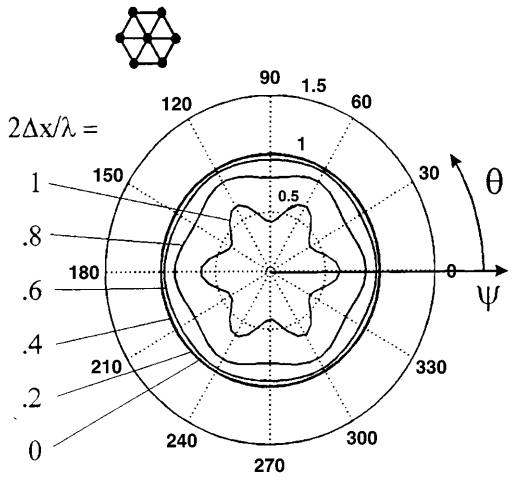

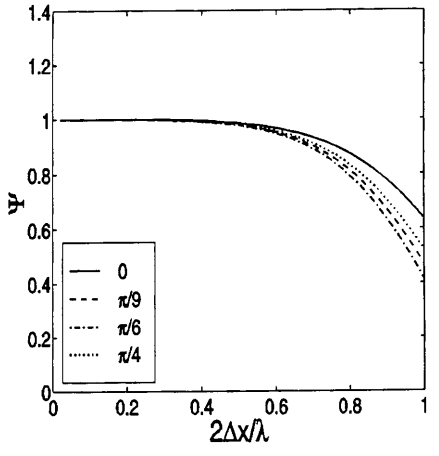

Fig. 13. FEM: Phase speed for the first-order wave equation with consistent mass matrix and hexagonal nodal configuration

quadrilateral nodal spacing and a consistent mass is about four times greater for FEM than for NEM (Figs. 16 and 17). The propagation through the FE triangles is highly anisotropic with the phase speed varying for the entire range of θ values. The periodicity is π and the largest error occurs along propagation direction parallel to the longest element side. NEM shows superior performance to that of linear FE. For the grids shown, the element orientation (especially the direction of the longest side of the triangle) is significant for the FE analyses. This dependence is not observed for NEM. Rotating the grid by $\pi/2$ causes no change in the NEM results, but does change the phase speed diagram for FEM.

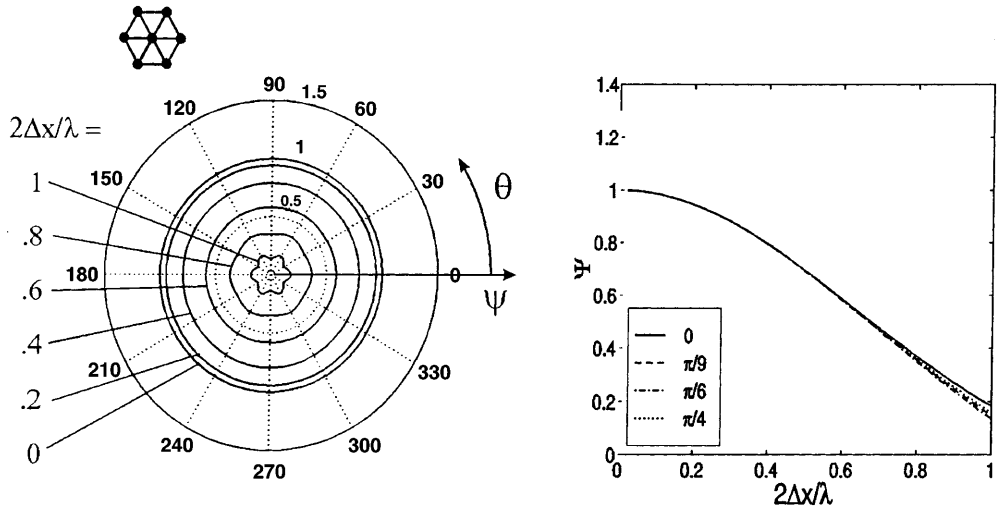

Fig. 14. NEM: Phase speed for the first-order wave equation with lumped mass matrix and hexagonal nodal configuration

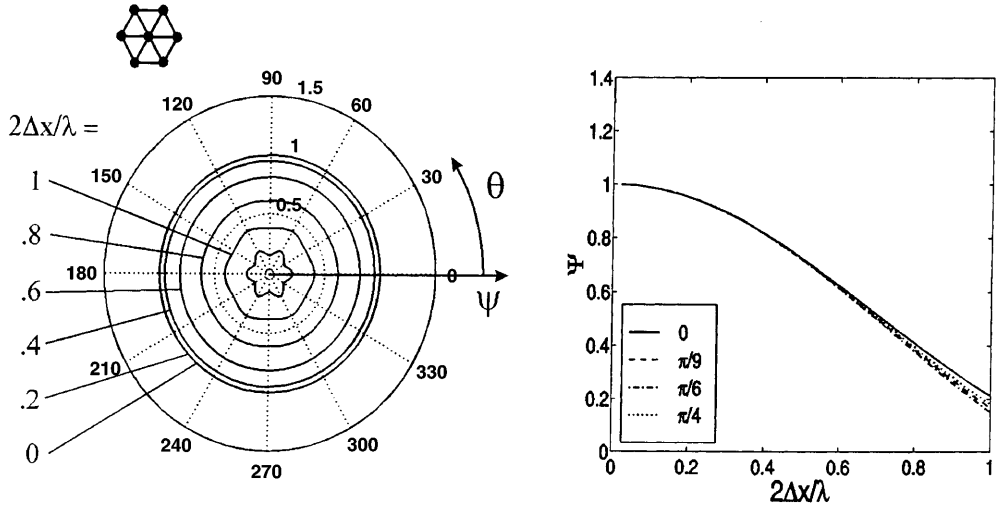

Fig. 15. FEM: Phase speed for the first-order wave equation with lumped mass matrix and hexagonal nodal configuration

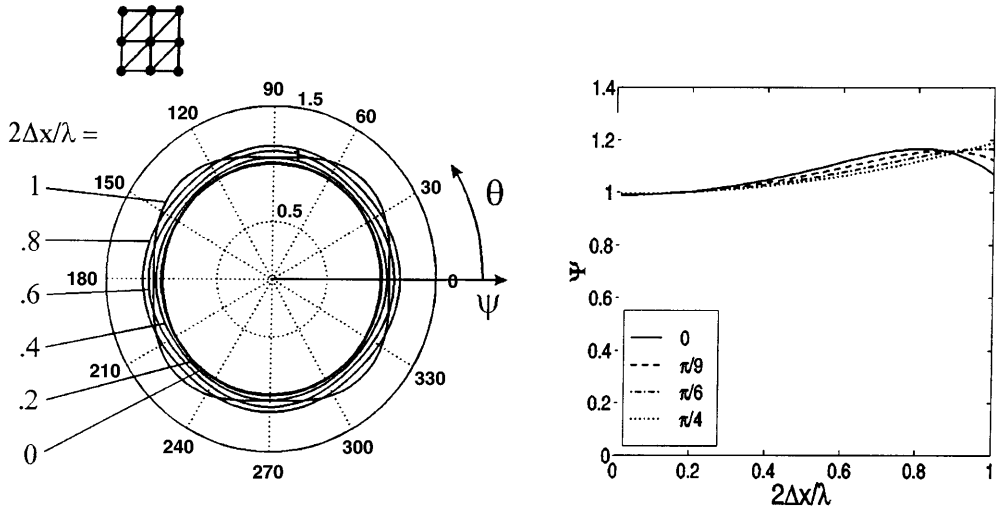

Fig. 16. NEM: Phase speed for the second-order wave equation with consistent mass matrix and quadrilateral nodal configuration

Hexagonal nodal spacing leads to excellent wave propagation for consistent mass matrix (Fig. 20). A phase speed error of less than 3 per cent is obtained for NEM with consistent mass, independent of the propagation direction. For the same case, FEM shows more than 20 per cent phase speed error (Fig. 21). But FEM performs marginally better than NEM for lumped mass matrices. The main advantage of hexagonal spacing is the better dispersive properties (small phase speed errors and near isotropic wave propagation) for lumped mass matrices (Figs. 22 and 23). For

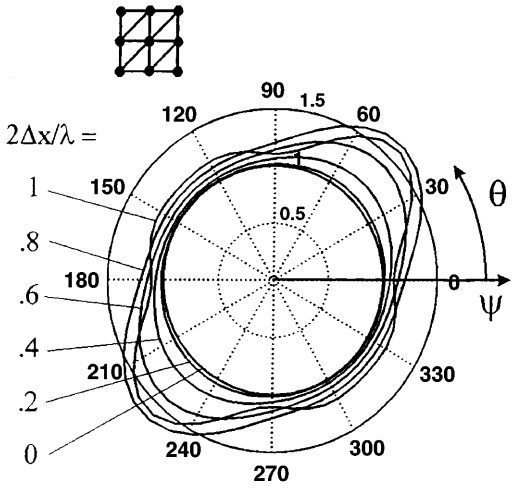

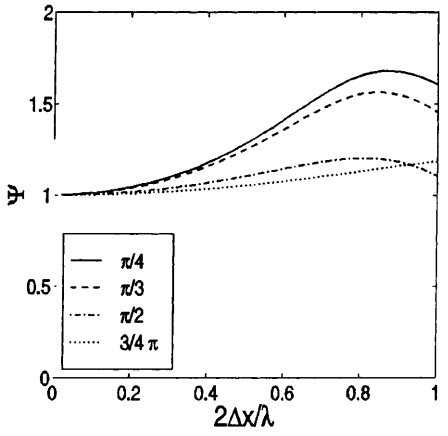

Fig. 17. FEM: Phase speed for the second-order wave equation with consistent mass matrix and quadrilateral nodal configuration

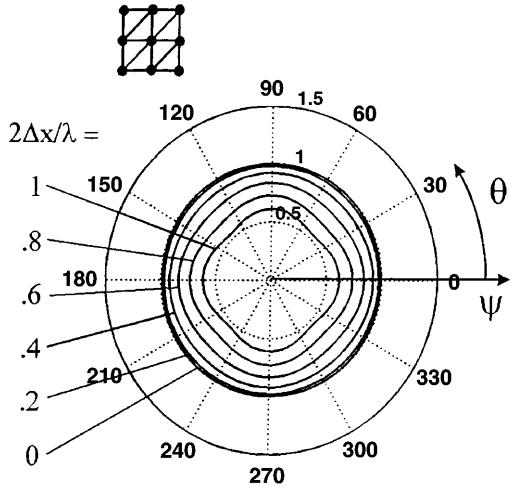

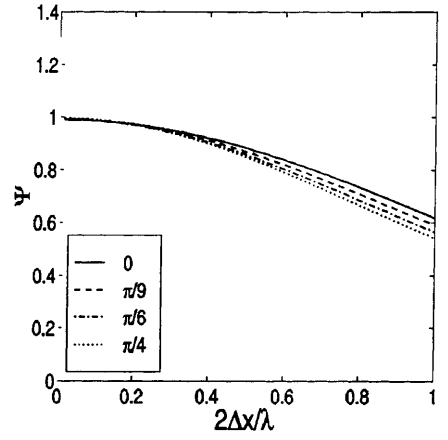

Fig. 18. NEM: Phase speed for the second-order wave equation with lumped mass matrix and quadrilateral nodal configuration

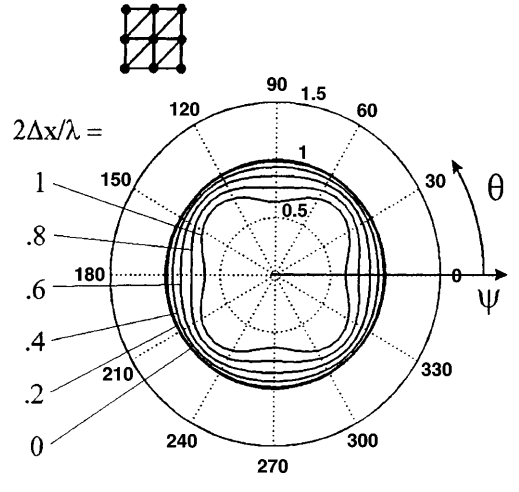

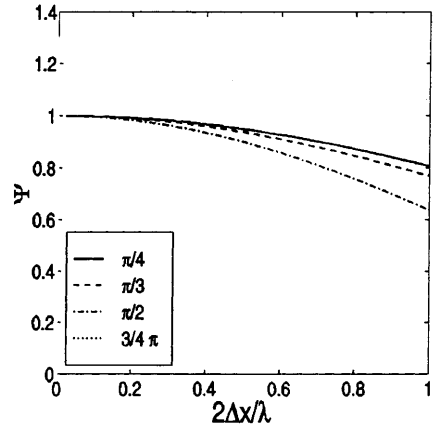

Fig. 19. FEM: Second-order wave equation with lumped mass matrix and quadrilateral nodal configuration

both FEM and NEM, the hexagonal nodal configuration performed better than the quadrilateral nodal grid, both in terms of reduced phase speed errors and less dependency on the propagation direction.

4.3.3
Optimization by higher order mass

A higher order (HO) mass matrix is obtained as a weighted sum of consistent (C) and lumped (L) mass matrices:

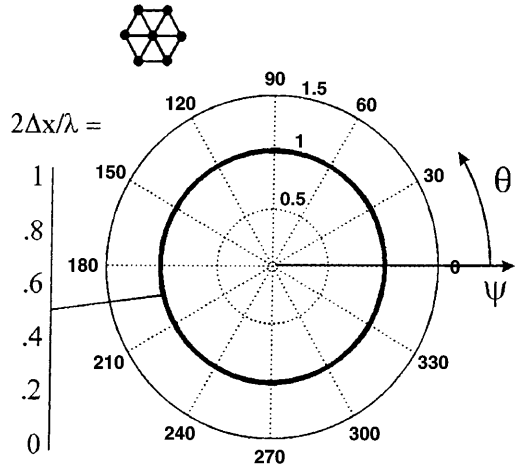

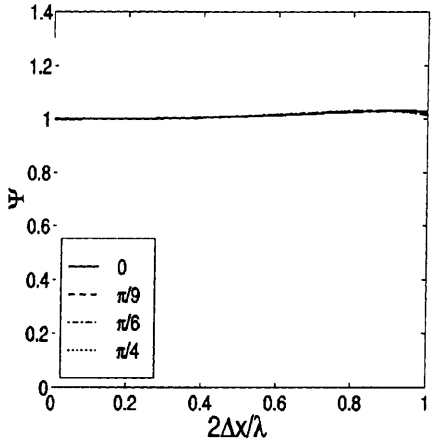

Fig. 20. NEM: Phase speed for the second-order wave equation with consistent mass matrix and hexagonal nodal configuration

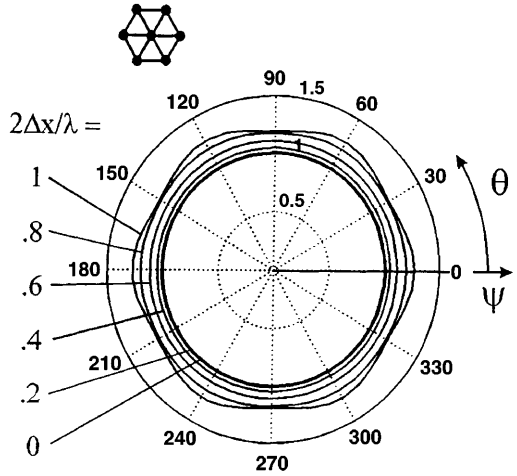

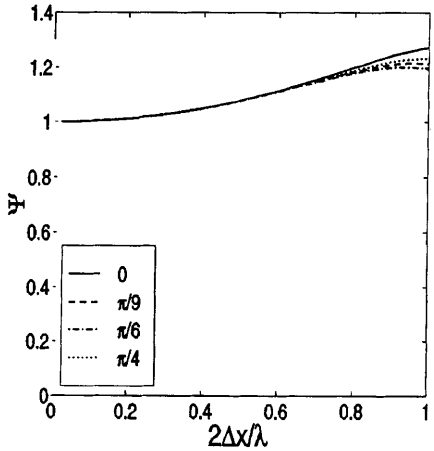

Fig. 21. FEM: Phase speed for the second-order wave equation with consistent mass matrix and hexagonal nodal configuration

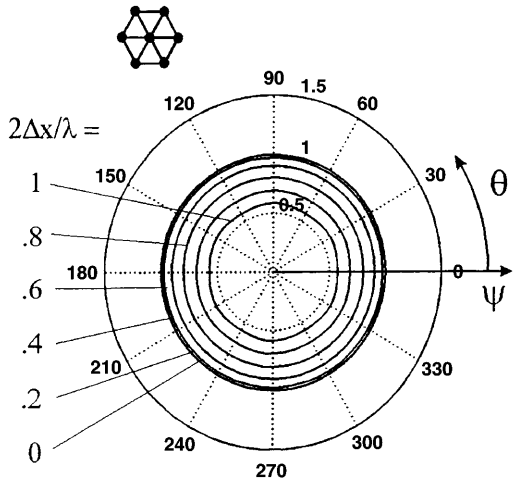

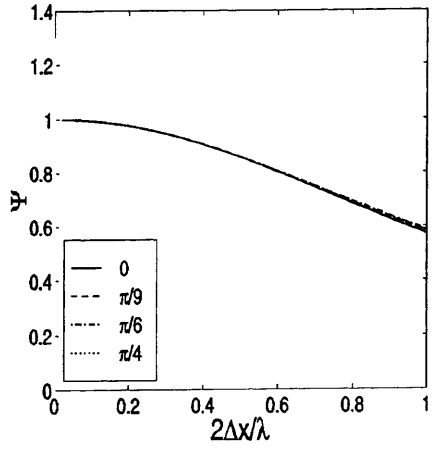

Fig. 22. NEM: Phase speed for the second-order wave equation with lumped mass matrix and hexagonal nodal configuration

$$\mathbf{M}^{\mathrm{HO}} = \alpha \mathbf{M}^{C} + (1-\alpha)\mathbf{M}^{L} \quad , \tag{22}$$

where α is the lumping parameter. For the first-order wave equation, lagging phase speeds are obtained for both, lumped and consistent mass matrices, with minimum phase speed error for the consistent mass. Hence, consistent masses show optimal performance.

The second order wave equation has leading and lagging phase speeds for consistent and lumped mass matrices, respectively. Hence, optimization is possible. The

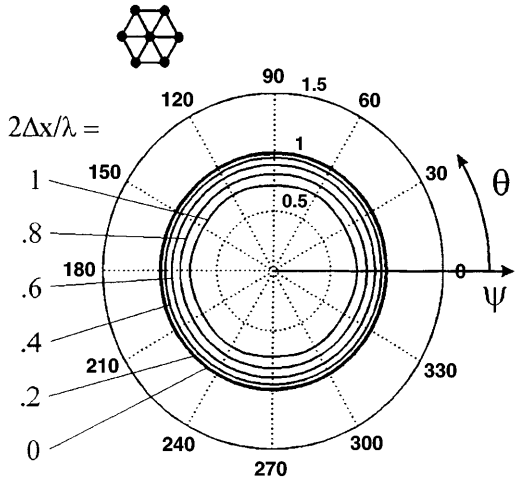

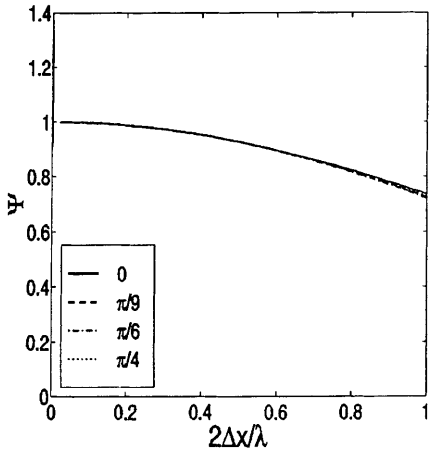

Fig. 23. FEM: Phase speed for the second-order wave equation with lumped mass matrix and hexagonal nodal configuration

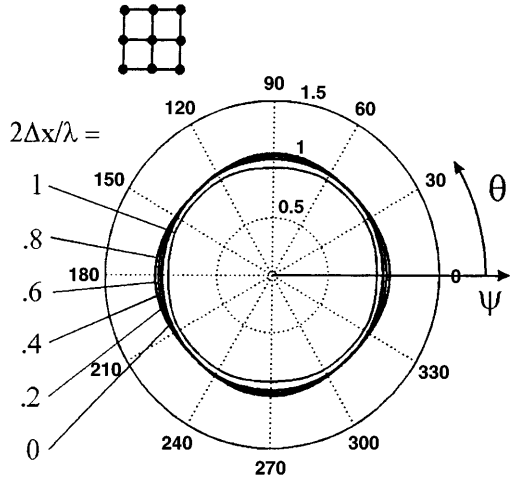

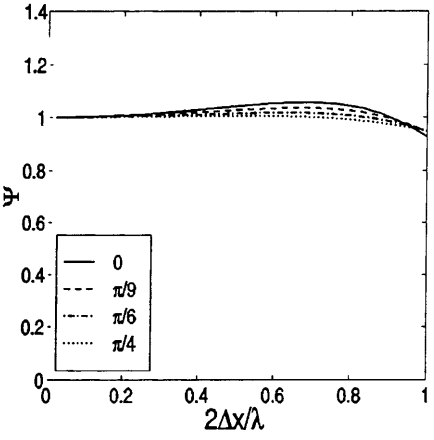

Fig. 24. NEM: Phase speed for the second-order wave equation with higher order mass matrix and quadrilateral nodal configuration

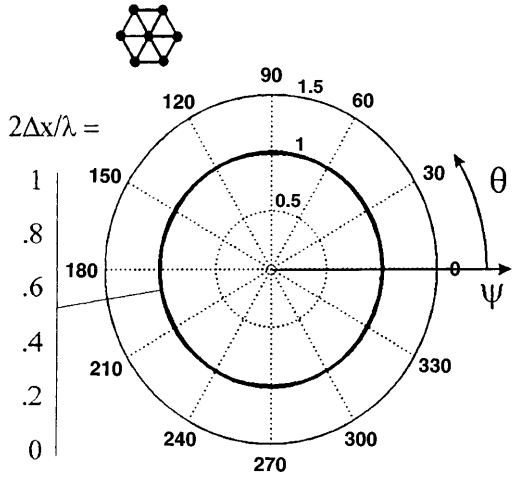

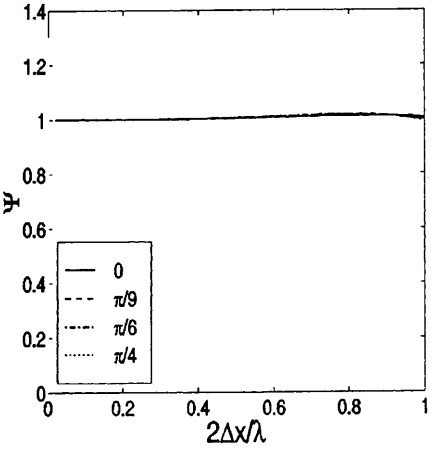

Fig. 25. NEM: Phase speed for the second-order wave equation with higher order mass matrix and hexagonal nodal configuration

minimum dispersion error for NEM with quadrilateral nodal configuration occurs at $\alpha = 0.85$. The results are shown in Fig. 24 with a phase speed error of less than 7 per cent. The hexagonal nodal configuration performs almost optimal for a consistent mass (Fig. 20). Slight improvement of the phase speed error is obtained for $\alpha = 0.98$. The maximum error in the phase speed reduces to 1.8 per cent, as can be seen in Fig. 25.

4.3.4
Summary

A dispersion analysis was carried out using NEM for first- and second-order wave equations. The performance of the NEM was compared to that for linear FE triangles. For the first-order wave equation, a lumped mass matrix gave near isotropic wave propagation but with greater phase speed error in comparison to the consistent mass matrix results. The NEM semi-discretization results were better than those of FEM. Results of the second-order wave equation using NEM with consistent mass were superior to FEM with high accuracy for wave lengths down to $2\Delta x$ – three nodes per wavelength. Optimal behavior is found for hexagonal nodal spacing and a higher order mass matrix. Voth and Christon (1998) obtained poor performance for the meshless reproducing kernel semi-discretization with lumped mass matrices compared to their FE counterparts. This is not true for NEM and the first-order wave equation. For the second-order wave equation, NEM shows greater phase speed error than FEM, but less dependency on the propagation direction.

For certain meshes, finite element triangles produce two wave solutions due to acoustical (lower) and optical (higher) frequencies. This phenomenon was not observed for NEM. In triangular finite elements, the shape functions are dependent on the element shape. Given a nodal configuration, different element meshes are possible which lead to different dispersive properties using FE triangles (Mullen and Belytschko, 1982).

5
Conclusions

The application of the natural element method to linear elastodynamics was studied. Two applications were considered: a vibration analysis of a cantilever beam subjected to a step load; and the dispersion properties of the NEM semi-discretization. The NEM solution for the time period and the beam displacement showed good agreement with the analytical solution. For the beam problem, the performance of NEM was better than that of constant strain finite elements. Wave propagation properties of the NEM semi-discretization were examined by a dispersion analysis. For the first-order wave equation, a hexagonal nodal configuration with a consistent mass matrix leads to wave propagation which is nearly independent of propagation direction θ, with less than 1 per cent phase speed error for nodal grids of four to five nodes per wavelength. Optimal performance for NEM was obtained for the second-order wave equation with a consistent mass matrix. Slight improvements were observed for higher order masses with phase speed error of less than 1.8 per cent for hexagonal nodal spacing and three nodes per wavelength. The overall performance of NEM in linear elastodynamics was better than that of linear finite elements. This can be attributed to the smoothness and higher-order approximation of the NEM interpolant. In particular, the interpolant and its derivatives are continuous across Voronoi and integration cell boundaries unlike the finite element interpolants which suffer slope discontinuities across element edges.

References

Braun J, Sambridge M (1995) A nmerical method for solving partial differential equations on highly irregular evolving grids. Nature 376:655–660

Cannmo P, Runesson K, Ristinmaa M (1995) Modelling of plasticity and damage in a polycrystalline microstructure. Int. J. Plasticity 11(8):949–970

Cook RD, Malkus DS, Plesha ME (1989) Concepts and Applications of Finite Element Analysis. John Wiley and Sons, Inc., New York

Cruz ME, Patera AT (1982) Parallel Monte-Carlo finite-element procedure for the analysis of multicomponent random media. Int. J. Num. Meth. Eng. 18:11–29

Farin G (1990) Surfaces over Dirichlet tessellations. Computer Aided Geometric Design 7(1–4):281–292

Ghosh S, Mallett RL (1994) Voronoi cell finite elements. Computers and Structures 50(1):33–46

Hurty WC, Rubenstein MF (1964) Dynamics of Structures. Englewood Cliffs, New York: Prentice-Hall

Irons BM, Treharne C (1971) A bound theorem of eigenvalues and its practical applications. In: Proceedings of the 2nd Conference on Matrix Method in Structural Mechanics, Wright-Patterson AFB, Ohio

Isaacson E, Keller HB (1996) Analysis of Numerical Methods. John Wiley and Sons, Inc., New York

Mullen R, Belytschko T (1982) Dispersion analysis of finite element semi-discretisation of the two-dimensional wave equations. Int. J. Num. Meth. Eng. 18:11–29

Sibson R (1980) A vector identity for the Dirichlet tesselation. Mathematical Proceedings of the Cambridge Philosophical Society 87:151–155

Sukumar N (1998) The Natural Element Method in Solid Mechanics. Ph.D. thesis, Theoretical and Applied Mechanics, Northwestern University, Evanston, IL, USA

Sukumar N, Moran B (1999) C^1 natural neighbor interpolant for partial differential equations. Numerical Methods for Partial Differential Equations 15(4):417–447

Sukumar N, Moran B, Belytschko T (1998) The natural element method in solid mechanics. Int. J. Num. Meth. Eng. 43(5):839–887

Voth TE, Christon MA (1998) Results of Von Neumann analyses for reproducing kernel semi-discretizations. In: Fourth Congress on Computational Mechanics, Buenos Aires, Argentina

Watson DF (1992) Contouring: A Guide to the Analysis and Display of Spatial Data Oxford: Pergamon Press